HSP90 inhibition in the mouse spinal cord enhances opioid signaling by suppressing an AMPK-mediated negative feedback loop†

Katherin A. Gabriel[1] and John M. Streicher[1,2,*]

[1]Department of Pharmacology, College of Medicine, University of Arizona, Tucson AZ USA
[2]Comprehensive Pain and Addiction Center, University of Arizona, Tucson AZ USA
*Corresponding author. Email: jstreicher@arizona.edu

Abstract

Opioids and other agonists of the μ-opioid receptor are effective at managing acute pain, but their chronic use can lead to tolerance that limits their efficacy. We previously reported that inhibiting the chaperone protein HSP90 in the spinal cord of mice promotes the antinociceptive effects of opioids in a manner that involved increased activation of the kinase ERK. Here, we found that the underlying mechanism involves the relief of a negative feedback loop mediated by the kinase AMPK. Intrathecal treatment of male and female mice with the HSP90 inhibitor 17-AAG decreased the abundance of the β1 subunit of AMPK in the spinal cord. The antinociceptive effects of 17-AAG with morphine were suppressed by intrathecal administration of AMPK activators and enhanced by an AMPK inhibitor. Opioid treatment increased the abundance of phosphorylated AMPK in the dorsal horn of the spinal cord, where it colocalized with a neuronal marker and the neuropeptide CGRP. Knocking down AMPK in CGRP-positive neurons enhanced the antinociceptive effects of morphine and demonstrated that AMPK mediated the signal transduction between HSP90 inhibition and ERK activation. These data suggest that AMPK mediates an opioid-induced negative feedback loop in CGRP neurons of the spinal cord, and that this loop can be disabled by HSP90 inhibition to enhance the efficacy of opioids.

†This manuscript has been accepted for publication in *Science Signaling*. Please refer to the complete, copyedited version on record at https://www.science.org/journal/signaling.

Introduction

Opioid drugs, like morphine and fentanyl, are well-established for the treatment of acute pain, such as postsurgical pain. However, opioids are limited in their efficacy for some pain types, such as musculoskeletal pain (*1*), and are accompanied by various side effects that include constipation, respiratory depression, and addiction, highlighting the need to find new ways to improve opioid therapy. The prototypical analgesic opioid morphine exerts its analgesic effect through the G-protein coupled μ-opioid receptor (MOR) (*2*). Activation of MOR leads to inhibition of adenylyl cyclase by the $G_{\alpha i}$ subunit, thus decreasing cyclic adenosine monophosphate (cAMP) production, whereas the $G_{\beta/\gamma}$ subunit complex activates inwardly rectifying K^+ channels and blocks voltage-gated Ca^{2+} channels. This altogether decreases the release of excitatory neurotransmitters and hyperpolarizes post-synaptic neurons, leading to an overall decrease of nociceptive neuron activity (*3*). There are, however, other mediators of opioid signaling that might be used to improve opioid therapy. For example, the identification of β-arrestin as a protein that blocks analgesia and enhances side effects led to the development of opioid agonists that are biased against arrestin recruitment (*4, 5*).

Heat shock protein 90 (HSP90), a chaperone protein, was identified by our lab as a key molecular regulator of opioid signaling in the central nervous system, with the potential of minimizing opioid negative side effects while enhancing their analgesic effect (reviewed in (*6, 7*)). When HSP90 is inhibited intracerebroventricularly (brain) by 17-*N*-allylamino-17-demethoxygeldanamycin (17-AAG) in different murine pain models, systemic morphine effects are completely ablated through a decrease in the activity of ERK-MAPK pathway signaling (*8-10*). Conversely, when 17-AAG was administered intrathecally (spinal cord), morphine antinociception was enhanced (*11*). The proposed mechanism for this enhancement was through disinhibition of the kinase ERK, leading to the activation of the kinase RSK and the translation of new proteins (*11*). Thus, our group built a model whereby HSP90 suppresses ERK MAPK signaling in lamina I/II of the dorsal horn of the spinal cord to reduce morphine-induced antinociception (*11, 12*).

Given that HSP90 is a major chaperone protein that regulates protein folding, scaffold formation, and protein localization, we decided to further investigate other potential targets involved in the signaling cascade downstream of MOR in the spinal cord (*6*). Quantitative proteomics performed on mice treated with 17-AAG intrathecally gave us 206 differentially expressed protein targets, and among them was AMP-activated protein kinase (AMPK) (*11*). AMPK is a major metabolic regulator in every cell type that is believed to be influenced by HSP90 (*13*). AMPK has also been shown to reduce morphine tolerance in mice (*14, 15*). These reports combined with our proteomic data provide a reasonable premise to hypothesize that HSP90-AMPK regulates opioid anti-nociception in the spinal cord downstream of the MOR.

To test this hypothesis, we investigated AMPK signaling in the spinal cord before and after HSP90 inhibition using pharmacological activators and inhibitors, along with selective CRISPR gene editing. We found that AMPK has a previously uncharacterized role as a negative feedback inhibitor of opioid anti-nociception in the spinal cord, which is disabled by HSP90 inhibition in order to enhance opioid pain relief. We localized this AMPK activity to neurons expressing Calcitonin Gene-Related Peptide (CGRP) and found that AMPK specifically in these neurons mediated this negative feedback mechanism. We further placed AMPK above ERK in our signaling model, describing a MOR-AMPK-ERK pathway which is regulated by HSP90. This work enhances our understanding of opioid molecular signal transduction cascades in the spinal cord and could provide new targets to improve opioid-based therapy.

Results

AMPK blocks opioid-induced anti-nociception in the spinal cord, which is reversed by HSP90 inhibition

We previously demonstrated that HSP90 inhibition in the spinal cord by 17-AAG, a competitive inhibitor that binds to the N-terminal domain of HSP90, enhanced morphine-induced antinociception (*11*). Because HSP90 has a large variety of client proteins, and to fully understand the key molecular players involved in this process, we ran a quantitative proteomic analysis on the spinal cords of CD-1 mice treated with vehicle or 0.5 nmol of 17-AAG (*11*). Among the 206 proteins up- or downregulated in spinal cord, we identified AMPK, a trimeric kinase that binds to AMP and is activated by phosphorylation of Thr^{172} of the alpha subunit (**Fig. 1A**). The data revealed that AMPK subunit β-1 (AMPK) was downregulated by 26% (**Fig. 1A**). Previous studies have shown that the activation of AMPK β subunit is required for the phosphorylation of Thr^{172} in the catalytic α subunit of AMPK (*16*). HSP90 has been shown to bind to the γ subunit of AMPK with high affinity, in order to maintain its α catalytic activity (*13*). If decreased AMPK activity is linked to enhanced opioid pain relief, then this suggests that AMPK acts as a negative regulator of opioid signaling.

To test this hypothesis, male and female CD-1 mice were treated with intrathecally administered 17-AAG or vehicle 24 hrs before treatment with intrathecal AMPK activator 5-Aminoimidazole-4-carboxamide riboside (AICAR), followed 10 minutes later by morphine injection and a tail flick nociception assay. In line with our hypothesis, we found that AICAR treatment completely reversed the enhanced anti-nociception evoked by 17-AAG treatment, below that of Vehicle-treated controls (**Fig. 1B-C**). Control experiments with AICAR alone, without morphine, showed no impact on baseline behavioral responses (**fig. S1**). Interestingly, we identified a sex difference in the effect of AICAR treatment alone without HSP90 inhibition by 17-AAG. Female mice had no effect of AICAR alone, with anti-nociception the same as Vehicle-treated controls (**Fig. 1B**). In contrast, male mice treated with AICAR alone had suppressed anti-nociception, below Vehicle-treated mice, and the same as 17-AAG+AICAR treated mice (**Fig. 1C**). This sex difference was confirmed by directly comparing male and female responses to AICAR in the context of morphine treatment, which were significantly different (**fig. S2A**).

These results suggest that AMPK activation blocks opioid anti-nociception, and reverses the effects of HSP90 inhibition, with a sex difference in terms of baseline activity of AMPK without HSP90 inhibitor treatment.

To confirm these findings, we used a second AMPK activator, PT1, that binds to the β subunit with a different mechanism of action than AICAR (*17*). PT1 also reversed the enhanced morphine anti-nociception caused by HSP90 inhibition, further confirming our hypothesis that AMPK acts as a negative regulator of opioid pain relief (**Fig. 1D**). A PT1-alone control experiment with no morphine treatment did show a slight anti-nociceptive effect in tail flick pain, but that is the opposite effect of the anti-nociceptive suppression observed with morphine (**fig. S1**). However, unlike AICAR, PT1 did not drive anti-nociception below Vehicle-treated levels, nor did it have a sex difference in the effects of the drug. Thus, although confirming our basic hypothesis, there may be small mechanistic differences revealed by the slightly different effects of the two different AMPK activators.

Our hypothesis that AMPK acts as a negative regulator of opioid signaling implies that AMPK inhibition should enhance opioid pain relief. To test this aspect of our hypothesis, we used the AMPK inhibitor dorsomorphin. We found that dorsomorphin alone enhanced morphine anti-nociception to a slightly greater extent than HSP90 inhibition with 17-AAG (**Fig. 1E**). Dorsomorphin combined with 17-AAG did not further enhance morphine anti-nociception, suggesting that HSP90 inhibition may have already maximally blocked AMPK signaling. Dorsomorphin-alone controls with no morphine treatment showed no effect of the drug on baseline response (**fig. S1**). We also found no sex differences in the impact of this inhibitor treatment. This experiment further validates and confirms our hypothesis that AMPK acts as a negative regulator of opioid pain relief.

Because opioid signaling can differ in different pain models, we next tested if AMPK signaling had the same impact in the post-operative paw incision pain model. In line with our tail flick results, AMPK activation with both AICAR and PT1 led to a decrease in the enhanced antinociception caused by 17-AAG in the paw incision model (**Fig. 2, A and B**). AICAR also decreased morphine antinociception at baseline levels in males but not females, similar to the AICAR sex difference observed above (**Fig. 2A**). This was confirmed by direct comparison of the male and female response (**fig. S2B**). Unlike in tail flick pain, PT1 decreased anti-nociception below baseline Vehicle-treated levels, suggesting this pain model may be slightly more sensitive than the tail flick model (**Fig. 2B**). Lastly, when the AMPK inhibitor dorsomorphin was administered intrathecally, there was an enhancement of morphine anti-nociception similar to that caused by the HSP90 inhibitor 17-AAG (**Fig. 2C**). All 3 drugs were also tested alone, without morphine treatment, and none had any impact on the paw incision pain response (**fig. S1**). Overall, these findings are very similar to the tail flick results above, and further confirm that AMPK acts as a negative regulator of opioid signaling that is disabled by HSP90 inhibition.

DAMGO activates AMPK in the dorsal horn of the spinal cord, which is blocked by HSP90 inhibition

To contextualize the effect of HSP90 inhibition and opioid receptor activation on AMPK signaling in the spinal cord, we performed immunohistochemical (IHC) analysis on mice treated with 17-AAG with or without the high selectivity and efficacy MOR agonist DAMGO. We discovered that MOR activation with DAMGO caused an increase in AMPK phosphorylation, predominantly in the dorsal horn of the spinal cord (**Fig. 3A**). This signal was consistent with activation primarily in cell bodies and not processes such as dendrites or axons and occurred in both males and females.

We also observed an interesting sex difference in the way that males and females responded to HSP90 inhibition with 17-AAG. In males, combining DAMGO with 17-AAG caused an immediate and obvious loss of AMPK phosphorylation throughout the dorsal horn (**Fig. 3A**). In contrast, females still preserved AMPK phosphorylation after 17-AAG treatment (**Fig. 3A**). These results were confirmed by quantitation of our IHC data, finding that DAMGO stimulated AMPK phosphorylation in both males and females, but this stimulation was blocked by 17-AAG in males alone (**Fig. 3B**). This sex difference was confirmed by direct male and female comparison (**fig. S2C**). Overall, this analysis backs up our behavioral testing above, including the increased sensitivity of male mice to the effects of AICAR (**Figs. 1C and 2A**), and begins to place our observed AMPK signaling in a spinal circuit context.

DAMGO activates AMPK in peptidergic CGRP neurons in the dorsal horn of the spinal cord

Nociceptors, or neurons that detect and convey pain stimuli, are primary afferent nerve fibers that synapse in the dorsal horn of the spinal cord and are divided into two major classes: peptidergic and nonpeptidergic (*18*). Given that AMPK was activated predominantly in the dorsal horn in response to DAMGO, we performed colocalization studies to identify the AMPK neuron type. We used the neuronal cell body marker neuronal nuclei (NeuN), the nonpeptidergic primary afferent sensory neuron marker isolectin B4 (IB4), and the peptidergic nociceptor marker calcitonin gene-related peptide (CGRP). We chose CGRP because it contributes to pain transmission and inflammation; as well, its release from primary sensory neurons suggests it may be used as a peptidergic nociceptor marker (*19, 20*). Likewise, IB4-expressing neurons are involved in mechanical hyperalgesia (*21, 22*). We first found that phospho-AMPK signal widely overlapped with the NeuN marker, suggesting much of the AMPK activated signal is in neuronal cell bodies (**Fig. 4**). Furthermore, we observed significant co-localization with CGRP, linking MOR-AMPK signaling to these peptidergic nociceptive fibers. In contrast, we did not detect colocalization with IB4, suggesting no activation in nonpeptidergic fibers (**Fig. 4**). This was not a surprise given that CGRP is considered a pain-related substance and a key regulator of the development of morphine tolerance (*23*). This signifies that AMPK signal is activated by MOR in peptidergic neurons, which places this AMPK signaling in a circuit context.

Selective knockdown of AMPK in CGRP neurons

Although the above findings link MOR-AMPK signaling to CGRP neurons, they do not demonstrate the function of the AMPK signaling in that cellular context. We thus created a custom CRISPR/Cas9 construct to knockdown AMPK in CGRP-expressing neurons by placing the promoter of *Calca*, the gene expressing CGRP, in front of the *Cas9* gene (**Fig. 5A**). Mice were injected intrathecally with the CRISPR/Cas9 DNA constructs over the course of three days, and on day 10 they received morphine followed by the tail flick or paw incision assays (*9, 24*). Compared to the negative control (NC) CRISPR mice, the CGRP-AMPK CRISPR knockdown mice showed enhanced morphine antinociception in the tail flick assay (**Fig. 5B**). Similarly, the CGRP-AMPK knockdown treatment caused enhanced morphine anti-nociception in the paw incision assay (**Fig. 5C**). Of note, the apparent morphine response of the NC CRISPR mice appeared to be less than that in the previously shown vehicle-injected controls. We thus compared these mice directly and found that the morphine responses of the NC CRISPR mice were significantly reduced compared with that of the vehicle-injected mice (**fig. S3**). This small but significant decrease should be kept in mind when interpreting these data.

We validated successful target knockdown through immunohistochemical analysis of perfused spinal cords from mice treated with the NC CRISPR or the CGRP-AMPK CRISPR 10 min after intrathecal MOR activation with DAMGO. The Pearson correlation coefficient for overlap between the signals for phosphorylated AMPK and CGRP was reduced (notably to a level similar to that of random chance) in CGRP-AMPK CRISPR mice, demonstrating a loss of colocalization (**Fig. 5, D and E**). Phosphorylated AMPK and CGRP effectively colocalized in NC CRISPR mice but not CGRP-AMPK CRISPR mice, validating our model. Notably, we still observed substantial signal for phosphorylated AMPK in the CGRP-AMPK treated tissue, but it didn't correlate with that for CGRP. This shows that not all AMPK abundance was knocked down, just that in CGRP neurons. Overall, these results are consistent with a role for AMPK as a negative-feedback regulator of opioid signaling and pain relief, which our data links functionally to CGRP neurons. These results also suggest that HSP90 inhibition evokes its anti-nociceptive enhancement by decreasing AMPK activity in the soma of CGRP-expressing neurons.

An important caveat to note at this point is that this observation is correlative and does not definitively rule out AMPK activity elsewhere in the circuit. In particular, primary nociceptors innervating the dorsal horn from the periphery express the majority of CGRP in the spinal cord and could be a site of action. We especially cannot rule this out because we did not examine the dorsal root ganglia, to which intrathecal delivery of drugs and CRISPR constructs allows for diffusion. Similarly, our data cannot distinguish a pre-synaptic from a post-synaptic site of action for AMPK signaling.

AMPK signaling is upstream of ERK-MAPK signaling in the opioid signaling cascade

We previously demonstrated that ERK phosphorylation in response to acute opioid in the spinal cord was enabled by HSP90 inhibition with 17-AAG, leading to enhanced pain relief (*11*). We thus sought to place our

recently discovered AMPK signal transduction within this MOR-ERK cascade. We first used IHC studies on the spinal cords of mice treated with an NC CRISPR or CGRP-AMPK–targeted CRISPR to detect ERK phosphorylation. As expected, spinal cords from mice treated with the NC CRISPR combined with DAMGO showed no ERK phosphorylation (**Fig. 6A**). However, spinal cords from mice treated with the CGRP-AMPK CRISPR construct combined with DAMGO showed a strong activation of ERK phosphorylation in the superficial layers of the dorsal horn (**Fig. 6A**), much like we previously observed with 17-AAG and DAMGO treatment (*11*). This suggests that AMPK is upstream of ERK in the MOR-ERK cascade.

We further confirmed this finding using pharmacological treatments and Western blotting. First, we treated the mice with 17-AAG to enable ERK MAPK activation, followed by the AMPK activator PT1 and DAMGO. We found that DAMGO alone could stimulate ERK activation in spinal cord tissue after 17-AAG treatment (**Fig. 6B**), as we previously observed (*11*). In contrast, AMPK activation with PT1 completely blocked ERK activation by DAMGO (**Fig. 6B**), further confirming that AMPK is upstream of ERK and blocks ERK activation.

We also tested the converse using the AMPK inhibitor dorsomorphin without 17-AAG present. Without 17-AAG treatment, DAMGO could not stimulate ERK phosphorylation, as we previously observed (**Fig. 6C**, (*11*)). Dorsomorphin treatment by contrast enabled DAMGO to stimulate ERK phosphorylation (**Fig. 6C**). This finding further confirms that AMPK is upstream of ERK/MAPK and has a negative regulatory effect on ERK activation (and thus opioid-induced anti-nociception). Together, the results suggest that HSP90 maintains AMPK signaling in spinal CGRP neurons in response to acute opioid treatment as a negative feedback loop, which is disabled by HSP90 inhibition, leading to ERK signaling and enhanced opioid pain relief.

Discussion

In this study, we have identified AMPK as a key molecular regulator that acts as a negative feedback brake on opioid anti-nociception in the spinal cord (**Fig. 7**). In addition to this previously unidentified negative feedback mechanism through AMPK, other negative feedback signaling molecules and circuits have been identified that restrain opioid activity in both the brain and spinal cord. Work from our laboratory and others has shown that the mu and delta opioid receptors heterodimerize, and that this heterodimer reduces the anti-nociceptive effects of opioids (*25, 26*). Cholecystokinin neurons in the rostroventral medulla act as an “anti-opioid” system to reduce opioid-induced analgesia and enhance side effects (*27, 28*). Perhaps most relevant to this study, the ERK-MAPK pathway kinase c-RAF has been shown to promote hyperexcitability and reduce opioid activity in $IB4^+$ nociceptors (*29*). Our findings thus fit this general theme of negative feedback systems that evolved to balance and tune the activity of the endogenous opioid system.

Although these findings might seem contradictory to other literature reports that suggest that AMPK activation is beneficial in reducing pain and reducing morphine tolerance (*14, 30-32*), there are key differences in context

between them. First, AMPK activity in the context of pain transmission is different from AMPK activity downstream of MOR activation. For example, AMPK activity in microglia can reduce inflammatory activation and pain *(32)*, which is quite different from AMPK in CGRP neurons linking the MOR to effectors. We encountered an analogous situation with our ERK findings. Other reports link pain stimulus-induced ERK activation in the spinal cord with chronic pain development (*33*); however, this is different from ERK activity downstream of MOR activation, as we previously reported (*11*). Similarly, the reports linking AMPK activation to reduced morphine tolerance occur in the context of chronic opioid administration, which is a different context from the acute administration we explore here *(14, 31)*. Overall, these contrasting findings emphasize the importance of context in signal transduction. One signaling molecule does not have a unitary role in any particular process. That role depends on local organization of regulatory proteins, cellular location, and similar factors, all of which can differ with the same protein between cells, or within the same cell downstream of different signaling cascades (reviewed in (*6*)).

Notably, we uncovered some sex differences within our results. One of the AMPK agonists (AICAR) was effective in decreasing opioid-induced antinociception at baseline in male mice but not female mice, whereas an alternate AMPK activator PT1 was not different. We also found that HSP90 inhibition strongly decreased AMPK activation in the spinal cord in males but not in females. There have been some striking findings both in the clinic and pre-clinically about sex differences in pain transmission and response which could be contributing to this differential effect (*34*). Similarly, microglia have been implicated in the development of mechanical hypersensitivity in males but not females (*35*). Pain in females has been shown to be influenced by hormones, such as estradiol and prolactin, which can affect the way opioids respond overall (*36, 37*). These differences could also be due to different responses to the tools used; perhaps females have a different pharmacokinetic response to AICAR but not PT1. Understanding these sex differences is important and needs to be further explored to improve our understanding of opioid signaling in the spinal cord.

Another unanswered question is the mechanism through which HSP90 promotes AMPK signaling to limit morphine's anti-nociceptive effect. A previous report revealed that HSP90 can regulate the stability of AMPK phosphorylation and its overall kinase activity (*13*). This would explain why HSP90 inhibition with 17-AAG caused a decrease in overall AMPK expression and activity. Our lab has demonstrated that ERK can be activated as a response to acute opioids when HSP90 is inhibited, but the mechanism linking HSP90 to ERK had not been deciphered (*11*). Our results here from Western blotting and IHC analysis implicate AMPK as the link between HSP90 and ERK phosphorylation. However, this raises further questions. As a kinase, it's unlikely that AMPK-mediated phosphorylation of ERK would block ERK activity. It's more likely that AMPK activates an intermediary protein that goes on to deactivate or prevent the activation of ERK. One such candidate would be a phosphatase. Notably, AMPK was shown to activate a dual-specificity phosphatase (DUSP) to block ERK activation in carcinoma (*38*), and DUSP15 was shown to regulate the activation of ERK in Schwann cells (*39*), suggesting the potential for an HSP90-AMPK-DUSP-ERK signaling cascade in spinal cord. As well, the mechanism linking

ERK to enhanced anti-nociception is currently undetermined. Our earlier work suggested that protein translation downstream of ERK-RSK was necessary for enhanced anti-nociception (*11*). Although we still don't know the identity of the translated protein(s), the signaling cascade will need to converge on an ion channel, neurotransmitter transporter, or similar mechanism to regulate neuronal activity. We thus propose an investigation to identify such targets using our proteomic data set (*11*).

These findings also have potential clinical implications. AMPK agonists like metformin are heavily used for treating diabetes; this may be relevant for diabetic neuropathy patients, in which opioids tend to not work well (*40*). Blocking AMPK activity could be one way to circumvent this issue and enhance opioid efficacy, although the noted benefits for AMPK activation in pain and morphine tolerance should be kept in mind (*14, 41, 42*). Given the complexity of AMPK activity, it thus may make sense to pursue HSP90 inhibitor therapy as a means to enhance opioid pain relief. Several reports now have suggested that HSP90 inhibition can reduce neuropathic pain (*43-45*), and our own work suggests that spinal cord-localized HSP90 inhibition can boost the anti-nociceptive effect of opioids, establishing a basis for the use of HSP90 inhibitors as an opioid dose-reduction strategy (*11*) (reviewed in (*7*)). Thus, HSP90 inhibitors have potential as pain therapeutics, both to reduce pain and improve opioid-based therapy. Future work should further investigate this potential as well as the deeper and additional signaling mechanisms underlying opioid circuitry in the spinal cord.

Materials and Methods

Drugs

17-AAG (#AAJ66960MC), DAMGO (#11711), AICAR (#2840), Dorsomorphin dihydrochloride (#30-935-0), and PT1 (#40-392-5) were all purchased from Fisher Scientific (Waltham, MA). Morphine sulfate pentahydrate was obtained through the National Institute on Drug Abuse Drug Supply Program and distributed through the Research Triangle Institute. 17-AAG and PT1 were prepared as stock solutions in DMSO, and DAMGO, AICAR and Dorsomorphin dihydrochloride were prepared as stock solutions in water. Morphine was prepared fresh for each experiment in USP saline. Powders were stored as recommended by the manufacturer, and stock solutions stored at -20°C. Appropriate vehicle controls were used for each experiment: 10% DMSO in water for PT1, and 1% DMSO in water for 17-AAG i.t. injections; water for DAMGO, AICAR, and Dorsomorphin dihydrochloride i.t. injections; USP saline for systemic morphine injections. ‘

The dose of each drug used was based on literature reports and our previous work. For 17-AAG, we used a dose of 0.5 nmol i.t., selected from our previous dose/response experiment (*8*), and validated in spinal cord by the use of a second structurally-distinct HSP90 inhibitor (*11*). Dorsomorphin (also known as Compound C) was used at 20 nmol i.t., a similar but lower dose as previously reported in (*46*). AICAR was used at 100 nmol i.t., a

similar but slightly lower dose than in (*47*). We could not find any literature reports of i.t. or intracerebroventricular delivery of PT1, so we used a general starting dose of 10 nmol i.t., which we validated by comparison to our AICAR results. A DAMGO dose of 0.1 nmol i.t. and a morphine dose of 3.2 mg/kg subcutaneously (s.c.) are commonly used in the field, and in our previous work (*8, 11*).

CRISPR construct

A custom CRISPR gene editing construct was obtained from Genecopoeia as an all-in-one CRISPR clone with an sgRNA targeting both variants for mouse AMPK (*Prkaa1*) and the Cas9 gene, along with a neomycin resistance gene for mammalian cell selection and an mCherry gene for visualization (#CS-MCP001862-CG12-1-10, pCRISPR-CG12 vector backbone). The mouse CGRP (*Calca*) promoter (MPRM31284) was used to selectively drive expression of the Cas9 gene in CGRP-expressing cells. We also used a universal negative control (NC) vector that expresses all the same elements with a non-targeting sgRNA (#CCPCTR01-CG01-B). Each DNA vector was amplified for use using standard bacterial transformation, and an endotoxin-free maxi-prep kit to reduce inflammation upon injection.

Animals

Male and female CD-1 (also known as ICR) mice in age-matched controlled cohorts from 5 to 8 weeks of age were used for all experiments and were obtained from Charles River Laboratories (Wilmington, MA). Male and female mice were used in approximately equal numbers in each experiment; for the experiments where no sex differences were observed, male and female cohorts were combined for the data shown. CD-1 mice are commonly used in opioid research and in our previous work as a line with a strong response to opioid drugs (*8, 48*). Mice were recovered for a minimum of 5 days after shipment before being used in experiments. The mice were kept in an AAALAC-accredited vivarium at the University of Arizona under temperature control and 12-hour light/dark cycles with food (standard lab chow) and water available *ad libitum*. No more than five mice were kept in a cage. The animals were monitored daily, including after surgical procedures, by trained veterinary staff. All experiments performed were in accordance with IACUC-approved protocols at the University of Arizona and according to the guidelines of the NIH Care and Use of Laboratory Animals handbook.

Behavioral experiments

Prior to any behavioral experiment or testing, the animals were brought to the testing room in their home cages for at least 1 hour for acclimation. Testing always occurred within the same approximate time of day between experiments, and environmental factors (noise, personnel, and scents) were minimized. All testing apparatus (cylinders, grid boxes, etc.) were cleaned between uses. The experimenter was blinded to the treatment group by another laboratory member delivering coded drug vials, which were then decoded after collection of all data. Animals were randomly block assigned to treatment group by cage.

Paw incision and mechanical allodynia

Mechanical thresholds were determined prior to surgery using calibrated Von Frey filaments (Ugo Basile, Varese, Italy) with the up-down method and four measurements after the first response per mouse (*8, 49*). The mice were housed in a homemade apparatus with Plexiglas walls and ceiling and a wire mesh floor (3"W x 4"L x 3"H with 0.25" wire mesh). The surgery was then performed by anesthesia with ~2% isoflurane in standard air, preparation of the left plantar hind paw with iodine and 70% ethanol, and a 5-mm incision made through the skin and fascia with a no.11 scalpel. The muscle was elevated with curved forceps leaving the origin and insertion intact, and the muscle was split lengthwise using the scalpel. The wound was then closed with 5-0 polyglycolic acid sutures. All i.t. injections were performed as described in our previous work (*8*). For the 17-AAG experiments, the mice were injected i.t. and left to recover for 24 hours. The next day, the mechanical threshold was again determined as described above, and i.t. injections took place for the AICAR, PT1, and Dorsomorphin dihydrochloride experiments with a 10-min treatment time. The mice were then injected with 3.2 mg/kg morphine s.c., and mechanical thresholds were determined over a 3-hour time course.

For CRISPR experiments, 4.5 µg of DNA was complexed with GenJet plus reagent in vivo transfection reagent (#SL100500 from SignaGen) according to the manufacturer's instructions and injected i.t. daily from days 1 to 3. The mice then recovered, with the paw incision surgery performed on day 9 and opioid injection and pain measurement performed on day 10. Our in vivo CRISPR protocol is based on our protocol reported in (*9*). No animals were excluded from these studies.

Tail-flick assay

Pre-injection tail-flick baselines were determined in a 52 °C warm water tail-flick assay with a 10 sec cutoff time (*8*). The mice were then injected i.t. with 17-AAG or vehicle for 24 hours, then drug (AICAR, PT1, dorsomorphin dihydrochloride) or respective vehicle for 10 min. Baselines at 24 hours after injection were determined for the 17-AAG experiments. The mice were then injected s.c. with 3.2mg/kg of morphine, and tail-flick latencies were determined over a 2-hour time course. No animals were excluded from these studies.

For CRISPR experiments, 4.5 µg of DNA was complexed with GenJet plus reagent in vivo transfection reagent (#SL100500 from SignaGen) according to the manufacturer's instructions and injected i.t. daily from days 1 to 3. Behavioral measurements were taken on day 10 after a 3.2 mg/kg morphine s.c dose.

Western blotting and analysis

Mouse spinal cord protein lysates were prepared using our previously published protocol (*8*) and quantified with a BCA protein quantitation assay using the manufacturer's protocol (Bio-Rad). The protein was run on precast 10% Bis-Tris Bolt gels (Fisher Scientific #NW00100BOX) using the Bolt gel apparatus and following the

manufacturer's instructions. The gels were transferred to nitrocellulose membrane (Bio-Rad) using a wet transfer system (30 V, minimum of 1.5 hours on ice). The blots were blocked with 5% nonfat dry milk in TBS and incubated with primary antibody in 5% BSA in TBS + 0.1% Tween-20 (TBST) overnight rocking at 4°C. The blots were then washed three times for 5 min in TBST, incubated with secondary antibody (see below) in 5% milk in TBST for 1 hr of rocking at room temperature, washed again, and imaged with an Azure Sapphire infrared imaging system (Azure Biosystems, Dublin, CA). Some blots were then stripped with 25 mM glycine-HCl and 1% SDS, pH 2.0, for 30–60 min of rocking at room temperature prior to being washed and re-exposed to primary antibody. The resulting image bands were quantified using Scion Image (based on NIH Image). All images were quantified in the linear signal range, which is easier to ensure because the Azure imager is a dynamic imager that allows for fine control of exposure. The pERK signal was normalized to the tERK signal, with both measured from the same blot as the primary target. The normalized intensities were further normalized to a vehicle control present on the same blot.

Immunohistochemistry

Perfusions were performed on drug treated mice with cold PBS, followed with cold 4% paraformaldehyde in PBS. Shortly after the perfusions were complete, fixed spinal cords were extracted and immediately placed in cold 4% paraformaldehyde for ~6 hours. Spinal cords were then placed in 15% sucrose in PBS overnight, followed by 30% sucrose in PBS overnight. Spinal cords were then flash frozen in O.C.T. Compound using liquid nitrogen and sectioned with a Microm HM 525 cryostat at a thickness of 20 µm between the L5 and L6 vertebrae and mounted on Surgipath X-tra microscope slides. Spinal cord sections were rehydrated in PBS in preparation for free float staining. Samples were incubated in an endogenous peroxidase blocking buffer consisting of 60% methanol and 0.3% H2O2 in PBS at RT for 30 minutes and then washed with PBST. They were then incubated in 5% goat serum, 1% BSA in PBST at RT for 1 hour. Samples were then incubated with 1:200 primary pAMPK antibody in 1.5% goat serum, 1% BSA in PBST at 4℃ overnight. Samples were then washed with PBST and then incubated with a 1:200 Alexa Fluor goat anti-rabbit 488 in 5% goat serum, 1% BSA in PBST at RT for 1 hour in the dark. NeuN, IB4 and CGRP primary antibodies were used at 1:300, 1:200 and 1:200 respectively during the pAMPK primary incubation. The secondary for NeuN, IB4 and CGRP was Alexa Fluor goat anti-mouse 594 which was used at 1:200 for all three which was added during the pAMPK secondary incubation mentioned above. Stained spinal cord sections were then mounted onto slides with Novus FluorEver. Sections were imaged at 10x, 20x and 40x using an Olympus BX51 microscope equipped with a Hamamatsu C8484 digital camera. Images were analyzed using ImageJ. Dorsal horn regions were selected, and average mean intensities were measured and normalized to vehicle controls with an n=5 mice per group and each performed with 3 independent technical replicates.

Antibodies

The antibodies used were: pERK (Cell Signaling 4370S, lot 12, rabbit, 1:1000 for Westerns, 1:2000 for IHC), tERK (Cell Signaling 4696S, lot 16, mouse, 1:1000), pAMPK (Cell Signaling PA5-37821, lot 8, rabbit 1:300 IHC), pAMPK (Invitrogen, PA5-37821, lot XC3525642, 1:200 Colocalization IHC), anti-CGRP (Abcam ab81887, 1:200 for IHC), IB4 (Invitrogen I21412, 1:300 for IHC), NeuN (1:1000; Abcam, ab104224, lot GR3247200-1, mouse), secondary GαM680 (1:10,000; LI-COR, 926-68020, lot C50721-02, goat), secondary GαR800 (1:10,000; LI-COR, 926-32211, lot C50602-05, goat), secondary Alexa Fluor goat anti-mouse IgG 594 (1:500; Invitrogen, A11032, lot 1985396, mouse), secondary Alexa Fluor goat anti-mouse IgG 488 (Invitrogen A-11034, lot 2110499, rabbit, 1:200).

Statistical analysis

All data were reported as the mean ± SEM and normalized where appropriate as described above to total protein and/or Vehicle control groups. The behavioral data were reported raw without maximum possible effect (MPE) or other normalization. Biological and technical replicates are described in the Figure Legends. Comparisons between two groups (proteomic analysis, Pearson coefficient) were performed by unpaired two-tailed *t* tests. Behavioral data with a time course was compared using a Repeated Measures two-way ANOVA with a Sidak's (CRISPR data) or Dunnett's (all other data) *post hoc* test. Comparisons of the IHC and Western data were performed using a one-way ANOVA with a Tukey's *post hoc* test. In all cases, significance was defined as $p < 0.05$. All graphing and statistical analyses were performed using GraphPad Prism 8.3 (San Diego, CA). Males and females were included in every experiment and compared by two-way ANOVA. When different, they were reported separately, and when the data did not differ by sex, the male and female results were combined.

Supplementary Materials

Figures S1 - S3

References and Notes

1. J. M. Berthelot, C. Darrieutort-Lafitte, B. Le Goff, Y. Maugars, Strong opioids for noncancer pain due to musculoskeletal diseases: Not more effective than acetaminophen or NSAIDs. *Joint Bone Spine* **82**, 397-401 (2015).
2. C. Zöllner, C. Stein, Opioids. *analgesia*, 31-63 (2006).
3. R. Al-Hasani, M. R. Bruchas, Molecular mechanisms of opioid receptor-dependent signaling and behavior. *The Journal of the American Society of Anesthesiologists* **115**, 1363-1381 (2011).
4. C. L. Schmid *et al.*, Bias Factor and Therapeutic Window Correlate to Predict Safer Opioid Analgesics. *Cell* **171**, 1165-1175 e1113 (2017).
5. B. R. Varga, J. M. Streicher, S. Majumdar, Strategies towards safer opioid analgesics—A review of old and upcoming targets. *British journal of pharmacology*, (2021).

6. J. M. Streicher, The Role of Heat Shock Proteins in Regulating Receptor Signal Transduction. *Mol Pharmacol* **95**, 468-474 (2019).
7. J. M. Streicher, The role of heat shock protein 90 in regulating pain, opioid signaling, and opioid antinociception. *Vitam Horm* **111**, 91-103 (2019).
8. W. Lei *et al.*, Heat shock protein 90 (Hsp90) promotes opioid-induced anti-nociception by an ERK Mitogen Activated Protein Kinase (MAPK) mechanism in mouse brain. *J Biol Chem*, (2017).
9. W. Lei *et al.*, The Alpha Isoform of Heat Shock Protein 90 and the Co-chaperones p23 and Cdc37 Promote Opioid Anti-nociception in the Brain. *Front Mol Neurosci* **12**, 294 (2019).
10. C. Stine *et al.*, Heat shock protein 90 inhibitors block the anti-nociceptive effects of opioids in mouse chemotherapy-induced neuropathy and cancer bone pain models. *Pain*, (2020).
11. D. I. Duron *et al.*, Inhibition of Hsp90 in the spinal cord enhances the antinociceptive effects of morphine by activating an ERK-RSK pathway. *Sci. Signal.* **13**, (2020).
12. M. M. Heinricher, I. Tavares, J. L. Leith, B. M. Lumb, Descending control of nociception: Specificity, recruitment and plasticity. *Brain Res Rev* **60**, 214-225 (2009).
13. L. Zhang *et al.*, Hsp90 interacts with AMPK and mediates acetyl-CoA carboxylase phosphorylation. *Cellular Signalling* **24**, 859-865 (2012).
14. Y. Han *et al.*, Resveratrol reduces morphine tolerance by inhibiting microglial activation via AMPK signalling. *European Journal of Pain* **18**, 1458-1470 (2014).
15. S. Sanduja *et al.*, AMPK promotes tolerance to Ras pathway inhibition by activating autophagy. *Oncogene* **35**, 5295-5303 (2016).
16. J. S. Oakhill *et al.*, β-Subunit myristoylation is the gatekeeper for initiating metabolic stress sensing by AMP-activated protein kinase (AMPK). *Proceedings of the National Academy of Sciences* **107**, 19237-19241 (2010).
17. T. Pang *et al.*, Small molecule antagonizes autoinhibition and activates AMP-activated protein kinase in cells. *Journal of Biological Chemistry* **283**, 16051-16060 (2008).
18. A. I. Basbaum, Basic mechanisms. *Pain Management Secrets E-Book*, 19 (2009).
19. S. Benemei, P. Nicoletti, J. G. Capone, P. Geppetti, CGRP receptors in the control of pain and inflammation. *Current Opinion in Pharmacology* **9**, 9-14 (2009).
20. F. R. Nieto, A. K. Clark, J. Grist, V. Chapman, M. Malcangio, Calcitonin Gene-Related Peptide–Expressing Sensory Neurons and Spinal Microglial Reactivity Contribute to Pain States in Collagen-Induced Arthritis. *Arthritis & Rheumatology* **67**, 1668-1677 (2015).
21. P. Alvarez, X. Chen, O. Bogen, P. G. Green, J. D. Levine, IB4 (+) nociceptors mediate persistent muscle pain induced by GDNF. *Journal of Neurophysiology* **108**, 2545-2553 (2012).
22. E. K. Joseph, J. Levine, Hyperalgesic priming is restricted to isolectin B4-positive nociceptors. *Neuroscience* **169**, 431-435 (2010).

23. Z. Wang, W. Ma, J.-G. Chabot, R. Quirion, Calcitonin gene-related peptide as a regulator of neuronal CaMKII–CREB, microglial p38–NFκB and astroglial ERK–Stat1/3 cascades mediating the development of tolerance to morphine-induced analgesia. *Pain* **151**, 194-205 (2010).
24. A. J. Sandweiss *et al.*, Genetic and pharmacological antagonism of NK1 receptor prevents opiate abuse potential. *Mol Psychiatry*, (2017).
25. A. Keresztes *et al.*, Antagonism of the mu-delta opioid receptor heterodimer enhances opioid antinociception by activating Src and calcium/calmodulin-dependent protein kinase II signaling. *Pain*, (2021).
26. L. Milan-Lobo, J. Enquist, R. M. van Rijn, J. L. Whistler, Anti-analgesic effect of the mu/delta opioid receptor heteromer revealed by ligand-biased antagonism. *PloS one* **8**, e58362 (2013).
27. M. H. Ossipov, J. Lai, T. W. Vanderah, F. Porreca, Induction of pain facilitation by sustained opioid exposure: relationship to opioid antinociceptive tolerance. *Life Sci* **73**, 783-800 (2003).
28. T. M. Marshall *et al.*, Activation of descending pain-facilitatory pathways from the rostral ventromedial medulla by cholecystokinin elicits release of prostaglandin-E(2) in the spinal cord. *Pain* **153**, 86-94 (2012).
29. A. Garza Carbajal, A. Bavencoffe, E. T. Walters, C. W. Dessauer, Depolarization-Dependent C-Raf Signaling Promotes Hyperexcitability and Reduces Opioid Sensitivity of Isolated Nociceptors after Spinal Cord Injury. *J Neurosci* **40**, 6522-6535 (2020).
30. M. N. Asiedu, G. Dussor, T. J. Price, Targeting AMPK for the alleviation of pathological pain. In: M. Cordero, B. Viollet (eds), AMP-activated Protein Kinase. *Experientia Supplementum* **107**, 257-285, Springer, Cham. (2016). https://doi.org/10.1007/978-3-319-43589-3_11
31. Y. Pan *et al.*, Metformin reduces morphine tolerance by inhibiting microglial-mediated neuroinflammation. *Journal of Neuroinflammation* **13**, 1-12 (2016).
32. A. Ge, S. Wang, B. Miao, M. Yan, Effects of metformin on the expression of AMPK and STAT3 in the spinal dorsal horn of rats with neuropathic pain. *Molecular Medicine Reports* **17**, 5229-5237 (2018).
33. L. Daulhac *et al.*, Diabetes-induced mechanical hyperalgesia involves spinal mitogen-activated protein kinase activation in neurons and microglia via N-methyl-D-aspartate-dependent mechanisms. *Mol Pharmacol* **70**, 1246-1254 (2006).
34. S. A. Nasser, E. A. Afify, Sex differences in pain and opioid mediated antinociception: Modulatory role of gonadal hormones. *Life Sciences* **237**, 116926 (2019).
35. R. E. Sorge *et al.*, Different immune cells mediate mechanical pain hypersensitivity in male and female mice. *Nature neuroscience* **18**, 1081-1083 (2015).
36. Y. Ji, B. Tang, R. J. Traub, Spinal estrogen receptor alpha mediates estradiol-induced pronociception in a visceral pain model in the rat. *Pain* **152**, 1182-1191 (2011).
37. M. Patil *et al.*, Prolactin regulates pain responses via a female-selective nociceptor-specific mechanism. *iScience* **20**, 449-465 (2019).

38. M. J. Kim *et al.*, AMP-activated protein kinase antagonizes pro-apoptotic extracellular signal-regulated kinase activation by inducing dual-specificity protein phosphatases in response to glucose deprivation in HCT116 carcinoma. *J Biol Chem* **285**, 14617-14627 (2010).
39. J. F. Rodriguez-Molina *et al.*, Dual specificity phosphatase 15 regulates Erk activation in Schwann cells. *J Neurochem* **140**, 368-382 (2017).
40. M. Shaqura *et al.*, Reduced number, G protein coupling, and antinociceptive efficacy of spinal mu-opioid receptors in diabetic rats are reversed by nerve growth factor. *J Pain* **14**, 720-730 (2013).
41. D. V. Tillu *et al.*, Resveratrol engages AMPK to attenuate ERK and mTOR signaling in sensory neurons and inhibits incision-induced acute and chronic pain. *Mol Pain* **8**, 5 (2012).
42. Y. Pan *et al.*, Metformin reduces morphine tolerance by inhibiting microglial-mediated neuroinflammation. *J Neuroinflammation* **13**, 294 (2016).
43. M. R. Hutchinson *et al.*, Evidence for a role of heat shock protein-90 in toll like receptor 4 mediated pain enhancement in rats. *Neuroscience* **164**, 1821-1832 (2009).
44. S. S. Lewis *et al.*, Evidence that intrathecal morphine-3-glucuronide may cause pain enhancement via toll-like receptor 4/MD-2 and interleukin-1beta. *Neuroscience* **165**, 569-583 (2010).
45. M. J. Urban *et al.*, Inhibiting heat-shock protein 90 reverses sensory hypoalgesia in diabetic mice. *ASN Neuro* **2**, e00040 (2010).
46. Y. Gui *et al.*, Involvement of AMPK/SIRT1 pathway in anti-allodynic effect of troxerutin in CCI-induced neuropathic pain. *Eur J Pharmacol* **769**, 234-241 (2015).
47. Y. J. Liu *et al.*, Activation of AMP-activated protein kinase alpha1 mediates mislocalization of TDP-43 in amyotrophic lateral sclerosis. *Hum Mol Genet* **24**, 787-801 (2015).
48. R. H. Vekariya *et al.*, Synthesis and Structure-Activity Relationships of 5'-Aryl-14-alkoxypyridomorphinans: Identification of a mu Opioid Receptor Agonist/delta Opioid Receptor Antagonist Ligand with Systemic Antinociceptive Activity and Diminished Opioid Side Effects. *J Med Chem* **63**, 7663-7694 (2020).
49. S. R. Chaplan, F. W. Bach, J. W. Pogrel, J. M. Chung, T. L. Yaksh, Quantitative assessment of tactile allodynia in the rat paw. *J Neurosci Methods* **53**, 55-63 (1994).

Acknowledgments: We acknowledge the UA Comprehensive Pain and Addiction Center for sharing their behavioral resources. We also acknowledge Drs. Chiu-Hsieh Hsu and Tally Largent-Milnes of the UA Comprehensive Pain and Addiction Center for their expert consultation on statistical analysis and spinal CGRP neurons, respectively.

Funding: This work was supported by an Arizona Biomedical Research Commission New Investigator Award #ADHS18-198875, a National Institutes of Health grant R01DA052340, and institutional funds from the University of Arizona.

Author contributions: KAG co-formulated the initial idea for the project, designed and performed all experiments, analyzed the data, and co-wrote the manuscript. JMS co-formulated the initial idea for the project, collaborated on project and experimental design, supervised KAG in the performance of this work, secured funding for the work, and co-wrote the manuscript.

Competing interests: JMS is an equity holder in *Teleport Pharmaceuticals, LLC* and *Botanical Results, LLC*, but these companies are not Hsp90-related. The authors have no other relevant conflicts of interest to declare.

Data and materials availability: All data needed to evaluate the conclusions in the paper are present in the paper or the Supplementary Materials.

Figure legends

Figure 1: AMPK signaling suppresses opioid anti-nociception, which is reversed by HSP90 inhibition. (A) Left, diagram of the active AMPK protein complex, showing the α/β/γ ternary complex. The protein is activated by AMP binding to the γ subunit, leading to phosphorylation of Thr^{172} in the α subunit and subsequent activation. Right, proteomic quantification of the β1 subunit of AMPK in spinal cord of female CD-1 mice 24 hours after treatment with vehicle or 0.5 nmol 17-AAG (HSP90 inhibitor) intrathecally (i.t.). N=3 mice in each group. Ion intensity mass spectrometry counts for each group are reported and compared. * = $p < 0.05$ by unpaired 2-tailed *t* test. This suggests AMPK downregulation after HSP90 inhibitor treatment. Data taken from proteomic data set reported in (*11*). **(B to E)** Tail flick time course analysis in male and female CD-1 mice treated i.t. with vehicle or 0.5 nmol 17-AAG, followed 24 hours later by i.t. treatment with vehicle or AMPK activator (100 nmol, B and C; 10 nmol, D) or inhibitor (20 nmol, E) for 10 min, then subcutaneously with 3.2 mg/kg morphine. BL, baseline. Data are mean ± SEM, N (animals per group) is noted in each graph. Four technical replicates were performed for each experiment. *$P < 0.05$, **$P < 0.01$, ***$P < 0.001$, and **** $P < 0.0001$ vs. same time point in the Veh/Veh group by RM 2-Way ANOVA with Dunnett's *post hoc* test.

Figure 2: AMPK signaling suppresses opioid anti-nociception in post-surgical pain. (A to C) Mechanical allodynia was measured in male and female CD-1 mice after paw incision surgery was performed along with intrathecal injection of vehicle or 17-AAG (0.5 nmol) and, after 24 hours recovery, injected intrathecally with either AMPK activator AICAR (100 nmol, A) or PT1 (10 nmol, B) or AMPK inhibitor dorsomorphin (20 nmol, C), and 10 min later subcutaneously with morphine (3.2 mg/kg). Data are the mean ± SEM; N mice per group noted in the graphs. The experiments were performed with 3 technical replicates. *$P < 0.05$, **$P < 0.01$, ***$P < 0.001$, and **** $P < 0.0001$ vs. same time point Veh/Veh group by RM 2-Way ANOVA with Dunnett's *post hoc* test.

Figure 3: AMPK is activated in the dorsal horn of the spinal cord by opioid treatment, which is blocked by HSP90 inhibition in males. (A and B) AMPK phosphorylation (pAMPK, green) analyzed by IHC in dorsal horn tissue slices from male and female CD-1 mice injected intrathecally with vehicle or 0.5 nmol 17-AAG then 24 hours later with vehicle again or 0.1 nmol DAMGO and sacrificed 10 min later. Representative images are shown (A); arrows note punctate staining. Scale bars, 100 μm. Data for the signal intensity of pAMPK (B) are mean ± SEM from N=5 mice/group with 3 slices analyzed per mouse. **P* < 0.05, ***P* < 0.01, and ****P* < 0.001 vs. indicated group by one-way ANOVA with Tukey's *post hoc* test.

Figure 4: Localization of activated AMPK signaling to CGRP-expressing neurons in the dorsal horn of the spinal cord. IHC for phosphorylated AMPK (pAMPK), NeuN, CGRP, and IB4 in dorsal horn tissue from male and female CD-1 mice injected intrathecally with vehicle followed 24 hours later with 0.1 nmol DAMGO, sacrificed 10 min later. Representative images are shown, and Pearson correlation coefficients for colocalization (such as indicated by arrows) are mean ± SEM from N=3 mice per group and 3 slices per mouse. Scale bars, 100 μm. ***P* < 0.01 vs. NeuN group; $^{\#\#\#}P$ < 0.001 vs. CGRP group; both by one-way ANOVA with Tukey's *post hoc* test.

Figure 5: Selective CRISPR gene editing of AMPK in CGRP-expressing neurons enhances opioid anti-nociception. (A) Diagram of the CGRP-AMPK CRISPR construct. The AMPK sgRNA is driven by a universal promoter U6, but the Cas9 protein is driven by the CGRP promoter (*Calca*). **(B)** Tail flick time course analysis in male and female CD-1 mice injected intrathecally with negative control (NC) CRISPR or CGRP-AMPK CRISPR constructs and, 10 days later, injected subcutaneously with 3.2 mg/kg morphine. BL, baseline. Data are mean ± SEM; N mice per group noted in the graph. Experiments were performed with 4 technical replicates. **P* < 0.05 and **** *P* < 0.0001 vs. same time point NC group by RM two-way ANOVA with Sidak's *post hoc* test. **(C)** Mechanical allodynia was measured in the CRISPR mice described in (B) with paw incision surgery one day before morphine treatment. Data are presented and analyzed as in (B), ****P* < 0.001 and **** *P* < 0.0001. **(D and E)** IHC analysis of pAMPK and CGRP colocalization in male and female CRISPR CD-1 mice as described in (B), with intrathecal 0.1 nmol DAMGO on day 10, and sacrificed 10 min later. Pearson correlation coefficients are mean ± SEM of N=3 mice per group, with 2 sections per mouse analyzed. *****P* < 0.0001 by unpaired two-tailed *t* test. Representative images are shown (E). Scale bars, 100 μm and (far right) 50 μm.

Figure 6: Placement of AMPK signaling upstream of ERK MAPK signaling in the MOR cascade. (A) IHC of phosphorylated ERK (pERK) in the spinal cord from male and female CD-1 mice injected intrathecally with

negative control (NC) CRISPR or CGRP-AMPK CRISPR constructs and, 10 days later, with 0.1 nmol DAMGO and sacrificed 10 min later. Images are representative of N=3 mice in each group, with 3 slices analyzed per mouse. Scale bars, 100 μm and, bottom 25 μm. **(B)** Western blotting for phosphorylated and total ERK in spinal cord tissue from male and female CD-1 mice injected intrathecally with vehicle or 0.5 nmol 17-AAG followed 24 hours later with vehicle or 10 nmol PT1 (AMPK activator), followed 10 min later with vehicle or 0.1 nmol DAMGO and sacrificed 10 min later. Analysis of pERK, normalized to total ERK in each sample then further normalized to the Veh/Veh group (set to 100), are mean ± SEM; N mice per group noted in the graphs. *$P < 0.05$ by one-way ANOVA with Tukey's *post hoc* test. **(C)** Western blotting for phosphorylated and total ERK in spinal cord tissue from male and female CD-1 mice injected intrathecally with vehicle or 20 nmol dorsomorphin (AMPK inhibitor) followed 10 min later with vehicle again or 0.1 nmol DAMGO, then sacrificed 10 min later. Analysis as in (B).

Figure 7: Summary model of MOR-HSP90-AMPK-ERK signal transduction cascade in spinal cord CGRP neurons. Activation of the MOR by morphine and other opioids stimulates AMPK signaling, which suppresses ERK activation by the MOR. This limits opioid anti-nociception. HSP90 maintains and promotes AMPK signaling, so when HSP90 is inhibited by 17-AAG, AMPK signaling is lost, and ERK stimulation by the MOR is enabled and opioid anti-nociception is increased. This cascade takes place in the context of CGRP neurons.

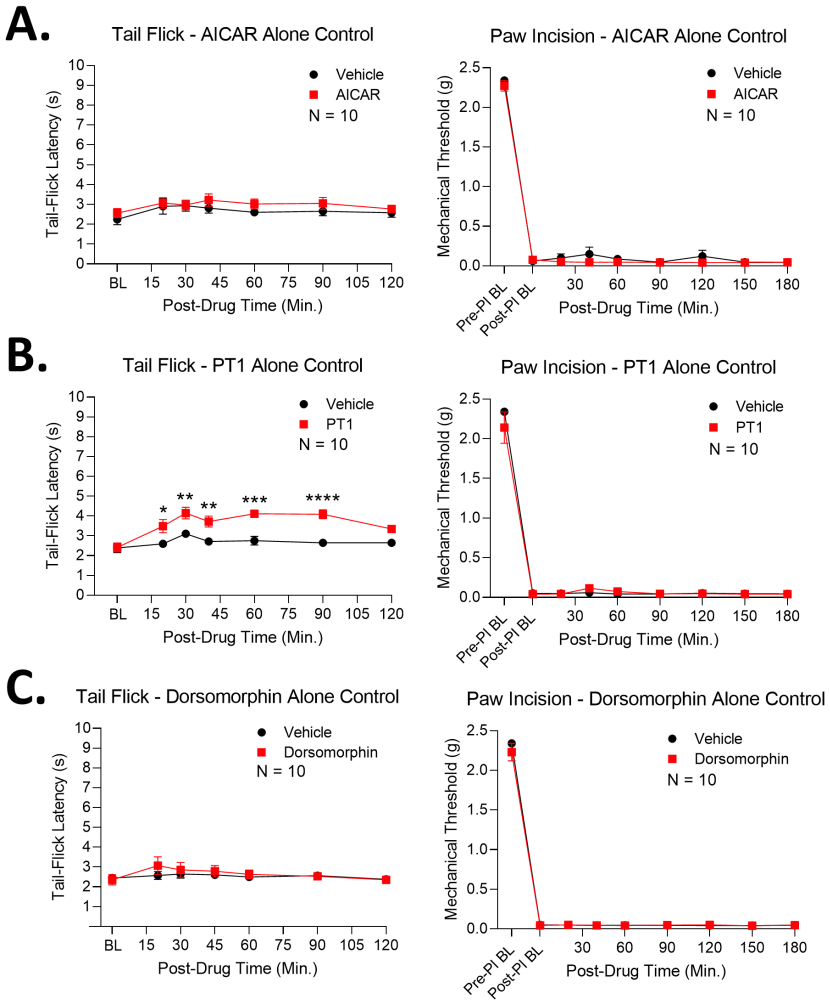

Figure S1: AMPK drug-alone controls. (A-C) Male and female CD-1 mice tested for any changes in pain response to the AMPK drugs used alone, with no morphine treatment. Tail flick (each panel, left) was performed at 52°C with a 10 sec. cutoff. Paw incision (each panel, right) was performed as described in the *Methods* with a 24-hour post-surgical recovery, and a time course analysis of mechanical allodynia was measured using von Frey filaments. Drug (100 nmol AICAR, A; 10 nmol PT1, B; 20 nmol dorsomorphin, C) or vehicle was injected intrathecally. Data are mean ± SEM; sample size (N, mice in each group) is noted in each graph. Each experiment comprised of 2 technical replicates. **P*< 0.05, ***P*< 0.01, ****P*< 0.001, and *****P*< 0.0001 vs. the same time point in the vehicle group by RM two-way ANOVA with Sidak's *post hoc* test.

Commented [SJM(1]: New Figure versions uploaded with bolding removed.

Deleted: and B

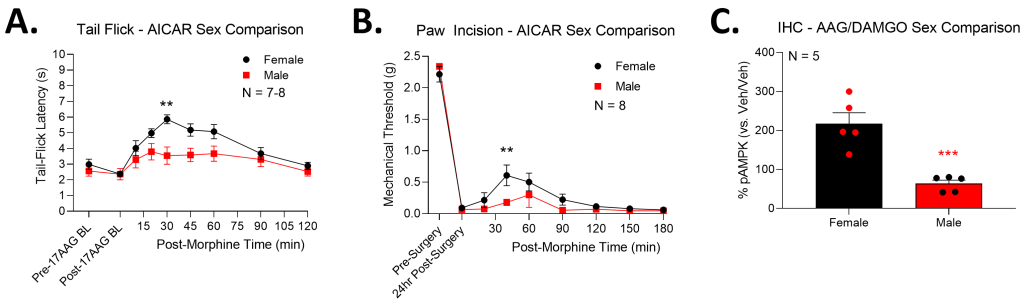

Figure S2: Confirmation of observed sex differences by direct comparison of male and female data. (A-B) Vehicle and AICAR group data from Fig. 1B-C (A) and Fig. 2A (B), directly compared. **(C)** IHC data from Fig. 3B directly compared. N noted in each graph. $^{**}P < 0.01$ by RM two-way ANOVA with Sidak's *post hoc* test (vs. same time point, A and B), and $^{***}P < 0.001$ by unpaired two-tailed *t* test (C).

Deleted: ,

Deleted: , and Fig. 3B (C)

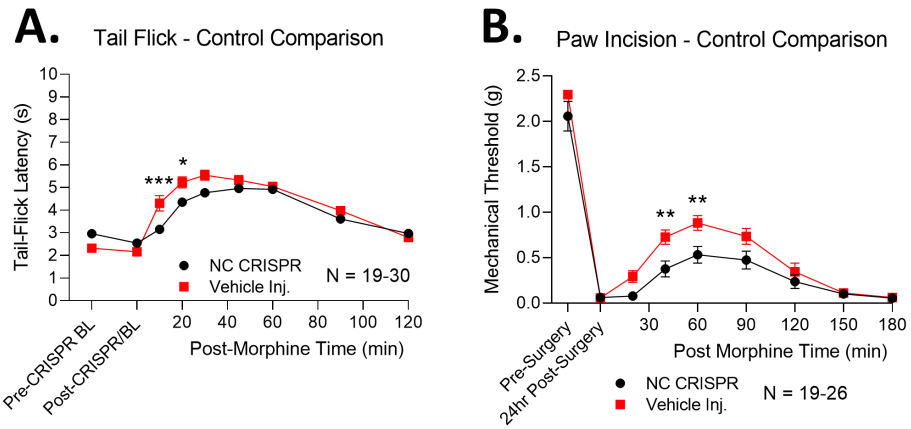

Figure S3: NC CRISPR control group demonstrates slightly lower morphine response than vehicle-injected controls. (A and B) NC CRISPR and vehicle/vehicle control data for all tail flick and paw incision mice collected from Figs. 1, 2, and 5 and combined for direct comparison. $^{*}P< 0.05$, $^{**}P< 0.01$, and $^{***}P< 0.001$ vs. the same time point in the NC CRISPR group by RM two-way ANOVA with Sidak's *post hoc* test.